

Kondo physics in tunable semiconductor nanowire quantum dots

Thomas Sand Jespersen,^{1*} Martin Aagesen¹, Claus Sørensen¹, Poul Erik Lindelof¹, Jesper Nygård¹

¹Nano-Science Center, Niels Bohr Institute,
University of Copenhagen, Universitetsparken 5, DK-2100
Copenhagen, Denmark

*To whom correspondence should be addressed; E-mail: tsand@fys.ku.dk.
(Dated: June 1, 2018)

We have observed the Kondo effect in strongly coupled semiconducting nanowire quantum dots. The devices are made from indium arsenide nanowires, grown by molecular beam epitaxy, and contacted by titanium leads. The device transparency can be tuned by changing the potential on a gate electrode, and for increasing transparencies the effects dominating the transport changes from Coulomb Blockade to Universal Conductance Fluctuations with Kondo physics appearing in the intermediate region.

As building blocks for quantum devices, semiconducting nanowires offer an appealing combination of properties not found in other systems. These properties include a wide range of material parameters of the nanowire itself (e.g. the vanishing nuclear spin of Si-nanowires or the high g -factor and strong spin-orbit coupling in InAs) and the wire geometry offering a wide choice of contact materials (e.g. superconductors or magnetic materials). Furthermore, nanowires offer the possibility of changing the crystal composition along the wire to facilitate e.g. tailored optical properties. In order to exploit these properties it is important to investigate basic quantum dot (QD) phenomena in nanowire devices and already, single electron transport has been demonstrated in weakly coupled nanowire quantum dots in the Coulomb Blockade (CB) regime [1, 2, 3] and Universal Conductance Fluctuations (UCF), Weak Localization and Anti-Localization [4] have been observed in low resistance nanowire devices. As a key example of a many-body effect in solid state physics, the Kondo effect in quantum dots has received considerable theoretical and experimental attention, but has so far remained elusive in nanowires partly because of the lack of barrier tunability. We here report on semiconducting nanowire devices with electrostatically tunable tunnel barriers, and the observation of the Kondo effect in the regime where the device acts as a strongly coupled quantum dot. We find that the Lande g -factor is significantly different from the bulk value for InAs due to the strong confinement of the wire. Moreover, indications of non-equilibrium Kondo effects are observed.

Our devices are based on semiconducting InAs-nanowires grown by molecular beam epitaxy (MBE) from *in-situ* deposited Au-catalyst particles. The wire diameters are ~ 70 nm and the lengths $2 - 5 \mu\text{m}$. These are the first measurements on MBE-grown InAs-nanowires and we expect that this well-established technique for growing ultra high quality III-V materials will produce wires of higher crystal quality and lower impurity concentrations than wires grown by other methods, thus resulting in cleaner systems for low temperature transport. Details on the

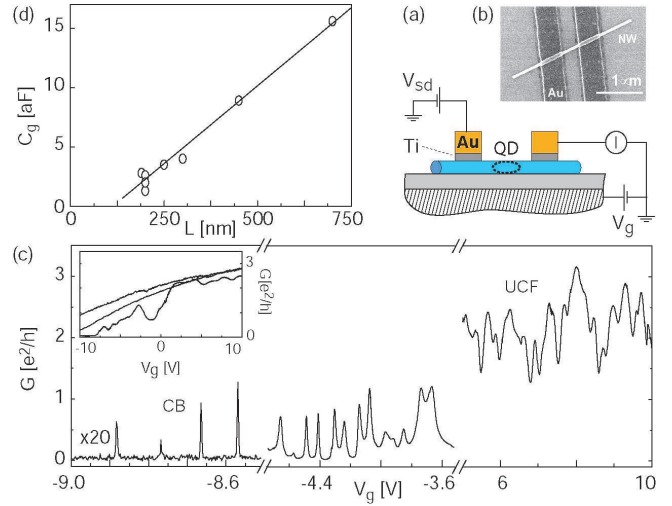


FIG. 1: (color online) (a) Side-view schematic of a nanowire quantum dot and the electrical setup. (b) A scanning electron micrograph showing a nanowire device with 300 nm electrode separation. (c) Linear conductance measurements $G(V_g)$ at $T = 0.3$ K and for temperatures $T = 270$ K, 130 K, 15 K (inset, top, middle, bottom curve). At 0.3 K and $V_g > 2$ V the contacts are open and UCF are observed. For -6 V $< V_g < -1$ V Kondo correlations are observed and for $V_g < -7$ V the device is dominated by CB. (d) QD-backgate capacitance C_g as a function of contact separation L .

growth and characterization of the wires will be published elsewhere [5]. The wires are transferred from the growth substrate to a highly doped Si-substrate with a 500 nm insulating SiO_2 cap-layer by gently pressing the two wafers together. By optical microscopy the wires are located with respect to predefined alignment marks and contacts are defined by E-beam lithography and subsequent evaporation of Ti/Au (10 nm/60 nm). To obtain clean metal-nanowire interfaces the devices are treated by a 10 sec. oxygen plasma etch followed by a 5 sec. wet etch in buffered hydrofluoric acid prior to metal evaporation. Omitting these last steps results in high resistance devices. Figure 1(a) shows a device schematic and

Fig. 1(b) a scanning electron micrograph of a typical device. The substrate acts as a back-gate electrode and for a given temperature T and external perpendicular magnetic field B the differential conductance dI/dV_{sd} is measured as a function of the applied source-drain voltage V_{sd} and back-gate potential V_g using standard lock-in methods.

Fig. 1(c) shows measurements of the linear response conductance G as a function of V_g at different temperatures for a device with $L = 200$ nm electrode separation. At room temperature (inset) the conductance varies monotonically from $0.9e^2/h$ at $V_g = -10$ V to $2.8e^2/h$ at $V_g = 10$ V thereby identifying the carriers as n -type (here e is the electron charge and h Planck's constant). At lower temperatures the slope of the $G(V_g)$ -trace increases but the conductance at $V_g = 10$ V remains effectively unchanged. This indicates a low barrier at the contacts at $V_g = 10$ V increasing with smaller gate-voltages. At 0.3 K (main panel), the behavior is as follows: For $V_g \lesssim -7.5$ V the device behaves as a quantum dot in the CB regime with large tunnel barriers between the leads and the dot with transport exhibiting sharp peaks separated by regions of zero conductance[6]. For $V_g \gtrsim 2$ V reproducible oscillations due to UCF are observed indicating low barriers between the leads and the QD. In the intermediate region the CB peaks are broadened due to a stronger coupling of the QD to the leads and Kondo physics emerges as discussed below. The periodic pattern of CB-peaks shows that the device behaves as a single dot rather than multiple dots in series[1]. The average peak separations $\Delta V_g \approx 80$ mV determine the capacitance from the dot to the back gate $C_g = e/\Delta V_g \sim 2$ aF and the linear dependence of C_g on the contact separation (Fig. 1.d) shows that the QD is defined by barriers at the contacts rather than defects along the wire which would result in random dot size fluctuations. The curve extrapolates to zero at $L_0 \approx 100$ nm suggesting a significant depleted region at the contacts. For metal contacts to bulk InAs it has been shown that the Fermi level pins in the conduction band (resulting in good electrical contact[7]), and assuming a similar behavior for InAs nanowires we believe that the QD is formed in the middle of the wire segment between the contacts due to the nonuniform electrical potential produced by the backgate and the grounded contacts.

We now focus on the intermediate gate-region of Fig. 1(c). Black and red traces of Fig. 2(a) show $G(V_g)$ for $T = 300$ mK and $T \approx 800$ mK, respectively and a series of broadened CB peaks are observed with each valley corresponding to a fixed number of electrons (N) on the dot. The non-zero valley conductance G_v indicate a significant contribution to the conductance from elastic co-tunneling processes exhibits an alternating pattern where high- G_v valleys are followed by valleys of lower G_v and vice versa. The even-odd pattern repeats in the addition energies (peak separations ΔV_g , see inset) suggesting a twofold degeneracy of the dot levels. The electron spin is

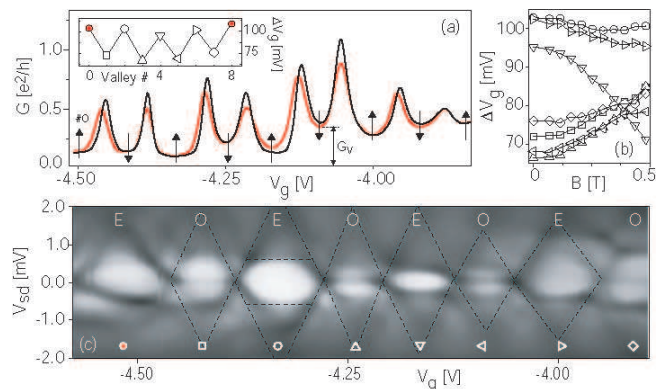


FIG. 2: (color online) (a) G vs. V_g for temperatures $T = 300$ mK (black) and $T \approx 800$ mK (red) showing overlapping CB-peaks. Alternating high/low valley conductance with corresponding decreasing/increasing behavior for increasing sample temperature (arrows) is observed. The peak spacings ΔV_g (inset) and their magnetic field dependence [panel (b)] follow a similar even-odd pattern. (d) Corresponding stability diagram [white/black] corresponds to $0e^2/h$ [$1.5e^2/h$] showing faintly visible CB-diamonds indicated by black lines and marked E/O according to even/odd electron occupation number N . A zero-bias Kondo resonance is observed through each odd- N CB diamond. The truncation of diamonds (horizontal features) indicate the onset of inelastic co-tunneling.

identified as the origin of this degeneracy by measuring the evolution of the peaks in a magnetic field as shown in Fig. 2(b). Valleys corresponding to odd(even) N are expected to widen(shrink) by the Zeeman splitting $g\mu_B B$ [8] (μ_B is the Bohr magneton) and this pairing behavior is readily observed. Figure 2(c) shows dI/dV_{sd} as a function of V_{sd} and V_g (stability diagram). A pattern of low conductance CB-diamonds (dashed lines), is visible, and the diamonds are numbered E/O according to even/odd N as determined from the magnetic field dependency. Pronounced conductance ridges at zero source-drain bias appear in every odd- N diamond. These observations are consistent with the Kondo effect: Whenever the dot holds an unpaired electron (odd N), its spin is screened by the conduction electrons in the contacts through multiple spin-flip tunnel events giving rise to a transport resonance at zero bias[9, 10]. When an even number of electrons reside on the dot the net spin is zero and no Kondo screening takes place.

In addition to the zero-bias resonances in the odd N diamonds the Kondo effect is distinguishable by unique magnetic field and temperature dependencies. The arrows in Fig. 2(a) indicate the temperature dependence of the valley conductance: In the absence of Kondo correlations (even N) G_v increases upon heating of the sample as for usual CB [6], but in odd- N valleys G_v decreases. The temperature dependence of a Kondo peak is described by the interpolation-function $G(T) = G_0(T_K'^2/(T^2 + T_K'^2))^s$. Here $T_K' = T_K/(2^{1/s} - 1)^{1/2}$ and $s = 0.22$ expected for a

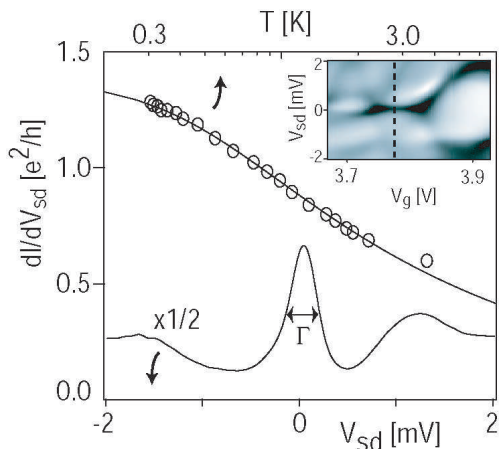


FIG. 3: Top curve: temperature dependence of the peak conductance for a particularly strong Kondo ridge. The solid line is a fit to the formula given in the text. The inset shows the stability diagram ($T = 300$ mK) and the lower curve shows dI/dV_{sd} vs. V_{sd} through the middle of the ridge (scaled by a factor of $1/2$).

spin-half system[11] and T_K is the so-called Kondo temperature. The inset to Fig. 3 shows a stability diagram measured in a different cool-down of the same device. A particularly strong Kondo resonance is observed and Fig. 3 shows dI/dV_{sd} vs. V_{sd} through the middle of the ridge at 300 mK (lower curve) and the valley conductance for different temperatures (upper curve). The solid line shows a fit to the formula above and the agreement is excellent yielding $T_K = 2.1$ K and $s = 0.22$ supporting the Kondo nature of the ridge. The Kondo temperature can also be estimated from the full width at half maximum $\Gamma \approx 2k_B T_k / e$ of the Kondo peak and for the data in Fig. 3 we find $\Gamma = 0.34$ mV and thus $T_K = \Gamma e / 2k_B = 2.2$ K in good agreement with the estimate above.

In a magnetic field the spin-degenerate states of the quantum dot are split by the Zeeman splitting $g\mu_B B$, which for Kondo resonances leads to peaks at $V_{sd} = \pm g\mu_B B / e$, independent of gate voltage[9]. The insets to Fig. 4(a) show stability diagrams of a Kondo ridge measured at zero field (left inset) and at $B = 0.5$ T (right). A gate independent splitting of the ridge is observed and the vertical traces through the middle of the diamond for magnetic fields of 0–0.9 T (Fig. 4(a)) shows the evolution of the splitting. Different methods for determining g from the splitting of the Kondo peak have been suggested in the literature. Refs. [12, 13, 14] suggest using the distance Δ_K between the peaks in dI/dV , however, for the weak coupling regime theoretical work has suggested the use of the distance δ_K between peaks in d^2I/dV^2 (steepest points in dI/dV_{sd})[15]. Figure 4(b) shows δ_K (open squares) and Δ_K (solid squares) extracted from the data of Fig. 4(a) and measurements at higher fields. Both Δ_K and δ_K show a clear linear dependence, and the param-

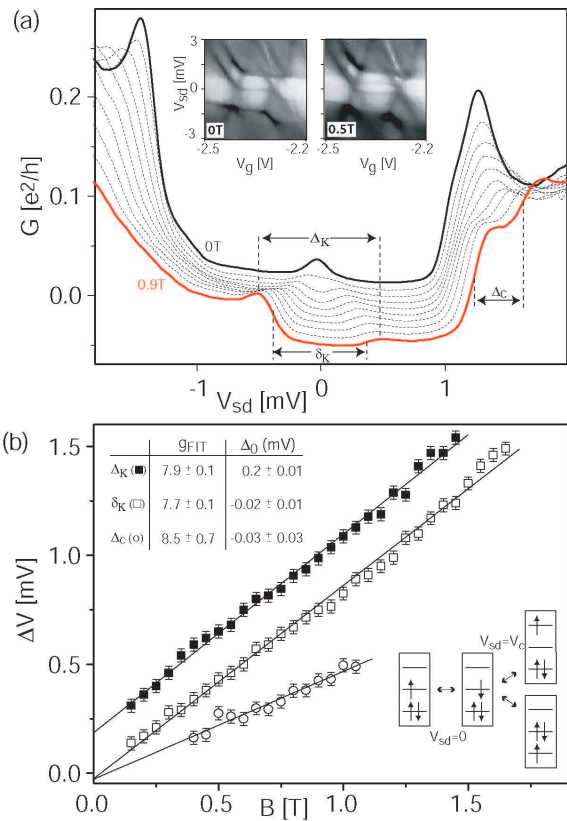


FIG. 4: (color online) (a) Stability diagrams at $B = 0$ T (left) and $B = 0.5$ T of an odd- N diamond with a Kondo resonance. Main panel shows traces through the middle of the diamond in magnetic fields of 0 T, 0.1 T, ..., 0.9 T (each offset by $-0.0075 e^2/h$). The peak at $V_{sd} \approx 1.25$ mV indicates the on-set of inelastic cotunneling. (b) The separation of the peaks in magnetic fields as indicated in (a). The upper inset shows the g -factor and extrapolated splitting Δ_0 at $B = 0$ T for the linear fits. (Right inset) Schematic diagram of cotunneling processes for zero source-drain bias (left) giving the usual Kondo effect, and at finite bias (right) yielding Kondo enhanced cotunneling peaks out of equilibrium. All states have total spin $S = 1/2$.

eters of the linear fits are shown in the inset with g calculated from the slope and Δ_0 the extrapolated splitting at $B = 0$ T. Both methods gives $g \approx 8$. The considerable downshift of the g -factor with respect to that of bulk InAs ($|g_{bulk}| = 15$) reflects the confinement of the nanowire geometry and agrees with measurements of g in InAs nanowire QD's in the CB-regime[16].

At a critical bias voltage $V_{sd} = V_c$ given by the excitation energy for the dot, inelastic cotunneling processes which leave the dot in an excited state set in, giving rise to horizontal ridges at finite bias within the Coulomb diamonds (Fig. 2(c) and Fig. 4). Figure 4(a) shows a sharp peak at zero field appearing at this onset ($V_c \approx 1.25$ mV), in addition to the zero bias Kondo peak (odd N). In a magnetic field the doublet excited state splits by $\Delta_c = g\mu_B B$, i.e. half that of the Kondo peak, allowing for an independent

estimate of g . The splitting is readily observed in Fig. 4(a) and the linear dependence of Δ_c vs. B (Fig. 4(b)) gives a g -factor of 8.5 ± 0.7 consistent with that measured from the Kondo peak.

We note that non-equilibrium population of the excited states at finite bias[15] may result in a broad cusp at the cotunneling on-set rather than a simple finite bias cotunneling step. This mechanism, however, cannot alone account for the peak in Fig. 4(a), being considerably narrower than the threshold bias and we propose that this peak is a signature of a Kondo resonance existing out of equilibrium. For carbon nanotubes, a detailed quantitative analysis recently showed that for an even N quantum dot inelastic cotunneling processes can result in a non-equilibrium singlet-triplet Kondo effect, accompanying transitions between the singlet ground state ($S = 0$) and an excited triplet state ($S = 1$)[17]. The Kondo correlations are in this case indicated by peaks at the cotunneling onset being narrower than the threshold bias. We see similar, sharp peaks in our devices in even N diamonds, however, for the odd N example in Fig. 4a, the effect coexists with the zero-bias Kondo effect and the cotunneling peak is intensified by (spin-flipping) transitions promoting the dot into excited states with the same total spin $S = 1/2$ as the ground state[20]. No theoretical models have been solved to allow for a quantitative description of this scenario, but presumably, the situation is readily achieved in other Kondo dot systems and it deserves theoretical attention.

The data illustrates that MBE grown InAs nanowires can constitute highly tunable quantum dots with a rich behavior, including strongly correlated electronic states and Kondo physics. Data from two devices is presented, however, the results are not unique to these: of the 9 devices investigated so far, the Kondo effect was observed in 4; the remaining 5 exhibiting only CB. Thus, given the recent advances in making superconducting contacts to nanowires[18] the present results show the promise of using nanowires for studying in a semiconductor system the interplay between two of the most pronounced many body effects in solid state physics: superconductivity and the Kondo effect. This subject has been experimentally addressable only in carbon nanotube based systems[19]. For helpful discussions we acknowledge K. Grove-Rasmussen, J. Paaske, C. Marcus, K. Flensberg, C. Flint, and E. Johnson.

Appl. Phys. Lett. **83**, 344 (2003).

- [2] Björk, M. T., Thelander, C., Hansen, A. E., Jensen, L. E., Larsson, M. W., Wallenberg, L. R., and Samuelson, L. *Nano Lett.* **4**, 1621 (2004).
- [3] Zhong, Z., Fang, Y., Lu, W., and Lieber, C. *Nano Lett.* **5**, 1143 (2005).
- [4] Hansen, A. E., Björk, M., Fasth, C., Thelander, C., and Samuelson, L. *Phys. Rev. B* **71**, 205328 (2005).
- [5] Aagesen, M. *et al.*, to be submitted.
- [6] Kouwenhoven, L., Marcus, C., McEuen, P., Tarucha, S., Westervelt, R., and Wingreen, N. In *Mesoscopic Electron Transport*, Sohn, L., Kouwenhoven, L., and Schön, G., editors, 105–214. Proceedings of the NATO Advanced Study Institute on Mesoscopic Electron Transport, (1997).
- [7] Bhargava, S., Blank, H., Narayanamurti, V., and Kroemer, H. *Appl. Phys. Lett.* **70**, 759 (1997).
- [8] Cobden, D. H., Bockrath, M., Mceuen, P. L., Rinzler, A. G., and Smalley, R. E. *Phys. Rev. Lett.* **81**, 681 (1998).
- [9] Glazman, L. and Pustilnik, M. *Low-temperature transport through a quantum dot*, H. Bouchiat *et al.*, eds. (Lectures notes of the Les Houches Summer School 2004), pp. 427-478. cond-mat/0501007.
- [10] Goldhaber-Gordon, D., Shtrikman, H., Mahalu, D., Abusch-Magder, D., Meirav, U., and Kastner, M. *Nature* **391**, 156 (1998).
- [11] Goldhaber-Gordon, D., Gores, J., Kastner, M. A., Shtrikman, H., Mahalu, D., and Meirav, U. *Phys. Rev. Lett.* **81**, 5225 (1998).
- [12] Kogan, A., Amasha, S., Goldhaber-Gordon, D., Granger, G., Kastner, M. A., and Shtrikman, H. *Phys. Rev. Lett.* **93**, 166602 (2004).
- [13] Cronenwett, S., Oosterkamp, T., and Kouwenhoven, L. *Science* **281**, 540 (1998).
- [14] Hewson, A. C., Bauer, J., and Koller, W. *Phys. Rev. B* **73**, 045117 (2006).
- [15] Paaske, J., Rosch, A., and Wolfle, P. *Phys. Rev. B* **69**, 155330 (2004).
- [16] Björk, M. T., Fuhrer, A., Hansen, A. E., Larsson, M. W., Froberg, L. E., and Samuelson, L. *Phys. Rev. B* **72**, 201307(R) (2005).
- [17] Paaske, J., Rosch, A., Wolfle, P., Mason, N., Marcus, C., and Nygård, J. *Nature Phys.* **2**, 460 (2006).
- [18] Doh, Y. J., van dam, J. A., Roest, A. L., Bakkers, E. P. A. M., Kouwenhoven, L. P., and De Franceschi, S. *Science* **309**, 272 (2005).
- [19] Buitelaar, M. R., Nussbaumer, T., and Schönenberger, C. *Phys. Rev. Lett.* **89**, 256801 (2002).
- [20] For a dot with nearly equidistantly spaced levels such as the region analyzed in Fig. 2(a) (insert), two different excited orbital states can contribute to this resonance, cf. the schematic in Fig. 4(b)

[1] De Franceschi, S., van Dam, J. A., Bakkers, E. P. A. M., Feiner, L. F., Gurevich, L., and Kouwenhoven, L. P.